THE JOURNAL OF PHYSICAL CHEMISTRY LETTERS
A JOURNAL OF THE AMERICAN CHEMICAL SOCIETY

pubs.acs.org/JPCL

Letter

Mapping Molecular Adsorption Configurations with <5 nm Spatial Resolution through Ambient Tip-Enhanced Raman Imaging

Matthew Gabel, Brian T. O'Callahan, Chloe Groome, Chih-Feng Wang, Regina Ragan, Yi Gu, and Patrick Z. El-Khoury*

Cite This: *J. Phys. Chem. Lett.* 2021, 12, 3586–3590

Read Online

ACCESS | Metrics & More | Article Recommendations | Supporting Information

ABSTRACT: We interrogate *para*-mercaptobenzoic acid (MBA) molecules chemisorbed onto plasmonic silver nanocubes through tip-enhanced Raman (TER) spectral nanoimaging. Through a detailed examination of the spectra, aided by correlation analysis and density functional theory calculations, we find that MBA chemisorbs onto the plasmonic particles with at least two distinct configurations: S- and CO_2-bound. High spatial resolution TER mapping allows us to distinguish between the distinct adsorption geometries with a pixel-limited (<5 nm) spatial resolution under ambient laboratory conditions.

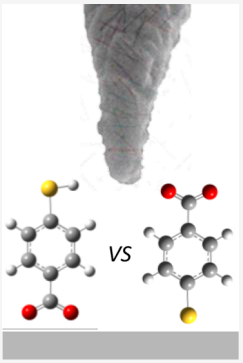

A plethora of physical and chemical phenomena contribute to plasmon-enhanced Raman spectra and images. Molecular reorientation/charging, Stark tuning, multipolar Raman scattering, vibronic/resonance effects, and plasmon-enhanced/induced chemical transformations are among the processes that come to mind in this context.[1] These effects complicate the analysis of surface- and/or tip-enhanced Raman (SERS[2] and TERS[3]) spectra and images, particularly when the goal of such measurements is to associate experimentally observed spectra with the formation of (photo)chemical reaction products at solid–air and solid–liquid interfaces.[4]

The above-mentioned physical and chemical processes lead to distinct and recognizable optical signatures, as described in a series of recent reports.[1] Generally, and in the limit of weak molecule–metal (and molecule–plasmon) coupling, modified relative intensity ratios in SERS and TERS can be associated with molecular reorientation and distinct surface selection rules (more on this in the ensuing sections).[5] New resonances, on the other hand, may arise from several phenomena, including (i) resonance (vibronic) Raman scattering,[6] (ii) multipolar Raman scattering,[7] (iii) molecular charging,[8] and (iv) chemical transformations.[9] The first can be avoided by using an incident laser frequency that does not coincide with an excited electronic state of the molecule. The second necessitates that the observed vibrations belong to the subset of molecular vibrations (both Raman allowed and Raman forbidden).[10] These can be both simulated and measured. Insights into the optical signatures of charged species can be gained from electrochemical Raman/SERS/TERS measurements.[11] Ideally, it is only once phenomena (i–iii) are established and understood that one can start exploring (photo)chemical transformations in the SERS and TERS schemes.[1]

A prototypical molecular reporter that has been extensively used to understand the effect of molecular orientation and conformation on SERS spectra is *p*-mercaptobenzoic acid (MBA). Previous work revealed that MBA adopts different adsorption configurations on silver, depending on the specific details of the procedures used for molecular deposition.[12] Particular emphasis was put on understanding how different concentrations and acidities affect the molecular configurations that MBA molecules adopt at the surface.[13] It was previously hypothesized that the carboxylate moiety of MBA features distinct configurations when deposited on silver colloids, including so-called flat, standing, and tilted orientations.[14] These various conformations naturally result in different intensity patterns in SERS. Very recently, Ghosh et al. combined ambient electrospray deposition with Raman spectroscopy (AESD RS) to map the evolution of the molecular orientation of *p*-MBA on silver nanoparticles.[15] The authors found that over time, there were sharp drops in certain peak intensities, which they associated with the reorientation of *p*-MBA molecules.

Received: March 1, 2021
Accepted: March 23, 2021
Published: April 5, 2021

https://doi.org/10.1021/acs.jpclett.1c00661
J. Phys. Chem. Lett. 2021, 12, 3586–3590

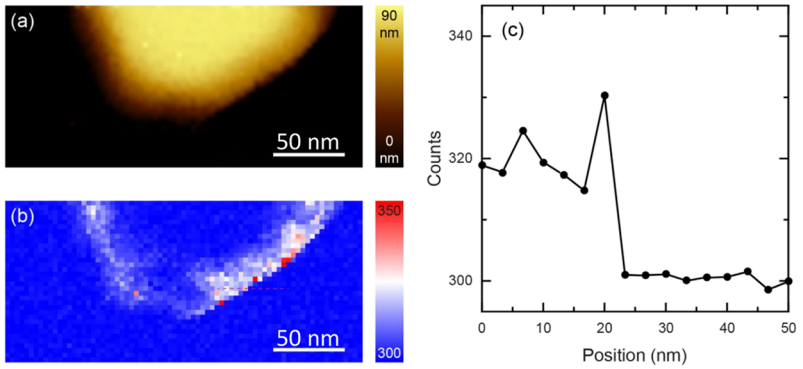

Figure 1. Concurrent AFM (a) and TERS (b) mapping of an MBA-coated silver nanocube. The TERS image is integrated in the 1557−1587 cm^{-1} spectral range. The dashed red line in (b) marks the positions at which the cross-sectional line profile in (c) was taken. The scale bars in (a) and (b) indicate 50 nm. Conditions used for TERS mapping: integration time = 0.5 s; power = 150 μW, focused using a 100×/NA = 0.7 objective; lateral step size ≈ 3.3 nm.

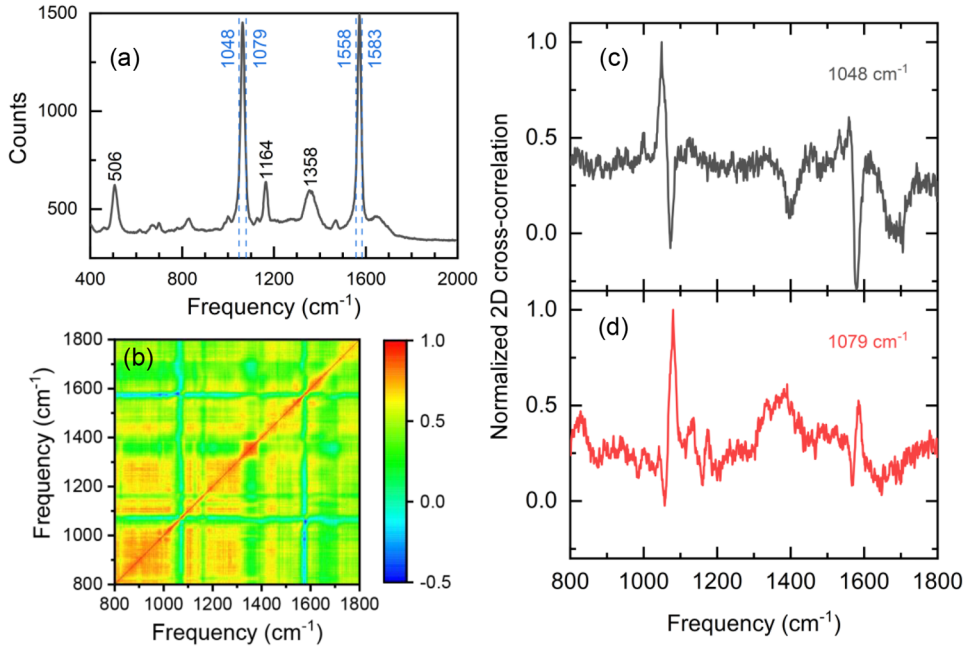

Figure 2. (a) Spatiotemporally averaged TERS response, taken from the data set shown in Figure 1b. A cross-correlation map ($\rho_{j,k} = \sigma^2_{jk}/\sigma_{jj}\cdot\sigma_{kk}$) of the spatially varying TERS spectra is shown in (b). Cross-correlation slices ($\nu_j \neq \nu_k$) are taken at two frequencies and shown in (c) and (d).

Herein, we revisit the enhanced Raman spectroscopy of MBA. We use TERS nanoimaging and nanospectroscopy in combination with correlation analysis and density functional theory calculations to gain additional insights into the binding motifs of silver-bound MBA. We capture two distinct binding geometries under our experimental conditions, best described as S- and CO_2-bound MBA. Notably, we demonstrate sub-5 nm spatial resolution in both chemical and adsorption configuration imaging under ambient laboratory conditions. We begin with a brief description of the recorded nanoimages.

Simultaneously recorded AFM (a) and TERS (b) maps of an MBA-coated silver nanocube are shown in Figure 1. The molecular response in the latter traces the structure of the local optical field in the TERS geometry, as previously established for silver nanocubes[5,16] and several plasmonic metal nanoparticles more generally.[1] The lateral step size used in these measurements is approximately 3.3 nm, as shown in Figure 1c. The same panel also shows that the attainable spatial resolution in our measurements is only limited by the pixel size. This is again consistent with prior reports from our group that addressed different molecular reporters on silver nanocubes via TERS, and where few nanometer spatial resolution in ambient TERS nanoimaging was demonstrated.[5,16]

Spatial averaging over TERS spectra recorded along the edges of several nanocubes yields the spectrum shown in Figure 2A. Peaks at 506, 1063, 1164, 1358, and 1572 cm^{-1} are visible in the spatiotemporally averaged response, which is consistent with prior SERS observations.[13] The TERS response is markedly different from the conventional Raman spectrum that was recorded from MBA powder (shown and discussed below). This is a result of the distinct configurations that MBA molecules adopt on silver, coupled with TERS selection rules that dictate that only incident/scattered radiation in the direction perpendicular to the substrate surface (along the tip axis) are enhanced. It is important to note that molecular orientation alone cannot explain our experimental observations. As shown in the Figure S1 of the Supporting Information section, *ab initio* molecular dynamics

https://doi.org/10.1021/acs.jpclett.1c00661
J. Phys. Chem. Lett. 2021, 12, 3586−3590

(AIMD)-based Raman spectral simulations that take both molecular orientation and TERS selection rules into account[17] cannot solely explain important features of our observations, e.g., the broad band at 1358 cm^{-1}. Rather, we will show that distinct binding motifs must be invoked to rationalize our experimental observations.

Prior to examining some of the theoretical Raman spectra of MBA, it is useful to determine the number of species that contribute to the TERS signal. We follow a recently outlined procedure,[18,19] which employs 2D correlation analysis to understand the correlations between the different peaks that contribute to the recorded optical response. The correlation map is shown in Figure 2b, whereas correlation slices taken at different resonances are shown in 2c, d. The cross-sectional correlation cuts may be used to infer the correlations between the different peaks we observe. Several observations in Figures 2c, d are worth highlighting. First, the 1063 and 1572 cm^{-1} peaks are in effect composed of 2 sets of correlated resonances: the first pair at 1048 and 1558 cm^{-1}, along with a second pair at 1079 and 1583 cm^{-1}. Second, the broad 1358 cm^{-1} signature is only correlated to the 1079 and 1583 cm^{-1} pair. It therefore appears that two distinct species, only one of which features a broad resonance at ∼1358 cm^{-1}, are responsible for the observed spectra.

We performed density functional theory calculations to shed light on the nature of the two species that we were able to isolate through correlation analysis. Figure 3 shows the

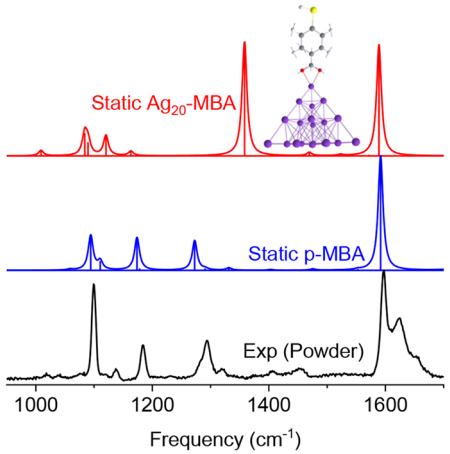

Figure 3. Experimental powder spectrum (black, 633 nm, 50 $\mu w/\mu m^2$) is shown along with the simulated spectra of the isolated (blue) and Ag_{20}-bound (red) MBA complex. The inset shows the structure of the CO_2−Ag bound complex.

experimental powder spectrum, the calculated spectra of the isolated MBA species as well as a singly deprotonated MBA molecule (carboxylate, not SH moiety) with its CO_2 group interacting with the apex of a cluster composed of 20 Ag atoms, denoted as Ag_{20}-MBA. The powder spectrum is reasonably well-reproduced *in silico* using the isolated MBA molecule. Note that models that emulate S−Ag binding (e.g., S-bound Ag-MBA, see Figure S2) yield a spectrum that is indistinguishable from the isolated MBA in the spectral region we probe in this work. The computed Raman spectrum of the CO_2-bound Ag_{20}-MBA model otherwise features an intense 1359 cm^{-1} band that can be assigned to the symmetric stretching of the CO_2 group that is interacting with the metal cluster. The position of the computed resonance is in excellent agreement with its experimental TERS analogue in Figure 2a. The broadening we observe in practice nonetheless suggests a broad distribution of molecular orientations. Overall, we can assign the two species identified above through correlation analysis with S−Ag bound (1048 and 1558 cm^{-1}) and CO_2−Ag bound (1079, 1358, 1583 cm^{-1}) MBA molecules.

Having established that at least two species contribute to the recorded TERS spectra, we now take a closer look at the optical response near the edge of the silver cube, see Figure 4. We identify a vertical cross-section, wherein the response alternates between the two spectra that we have assigned to the S- and CO_2-bound MBA species. The results show that we can resolve the (dis)appearance of one of the two forms with a pixel-limited spatial resolution (<5 nm). Notice that the appearance of the CO_2-bound form is marked by both the appearance of the 1358 cm^{-1} resonance as well as a marked increase in the intensities of the accompanying 1048 and 1558 cm^{-1} bands (Figure 4b). The latter-mentioned bands, however, are not clearly resolved from the corresponding 1079 and 1583 cm^{-1} resonances of the S-bound form, as shown in Figure 2. Overall, the demonstrated spatial resolution adds yet another data point to the set of high spatial resolution ambient TERS measurements that have recently appeared in literature.[1] These results are also reminiscent of our recently reported dual analyte TERS study,[21] in which two different molecules were discerned via TERS mapping with pixel-limited spatial resolution.

In conclusion, we recorded and analyzed the TERS spectral images of MBA molecules chemisorbed onto silver nanocubes. Several aspects of the recorded images are consistent with recently reported TERS maps of chemically functionalized plasmonic metal nanoparticles. The spectra, on the other hand, are rich in that they broadcast at least two different binding geometries of MBA on silver. We were able to dissect the spectra through a combination of correlation analysis and density functional theory calculations. Last, but not least, we demonstrate that our measurements can spatially resolve an individual adsorption configuration of MBA with pixel limited (<5 nm) spatial resolution under ambient laboratory conditions.

Finally, it is important to concede that by not probing the low frequency region of the spectrum (<400 cm^{-1}), we did not capture the modes that involve S−Ag stretching. An important consequence of the latter is our inability to experimentally preclude bidentate attachment for flat or near-flat adoption geometries, wherein both the S- and CO_2-moieties would be expected to bind with the substrate. More work is therefore warranted to better understand the 3D binding geometry of the CO_2-bound form under the experimental conditions used in this work.

METHODS

Silver nanocubes (d = 100 nm) were dropcasted onto silicon substrates and rinsed with ethanol. A small aliquot (2 mL) of a 2 mM ethanolic MBA solution was then dropcasted onto the sample and rinsed with excess amounts of ethanol prior to drying the resulting sample with N_2 gas.

Our TERS setup is described elsewhere in more detail.[5,20,21] Here, measurements were performed using silicon AFM tips (ATEC-FM) coated with 100 nm of either gold or silver. Spectra were recorded following 633 nm laser irradiation. The P-polarized 150 μW laser source was focused onto the sample using a 100×/NA = 0.7 air objective. The signal was collected

https://doi.org/10.1021/acs.jpclett.1c00661
J. Phys. Chem. Lett. 2021, 12, 3586−3590

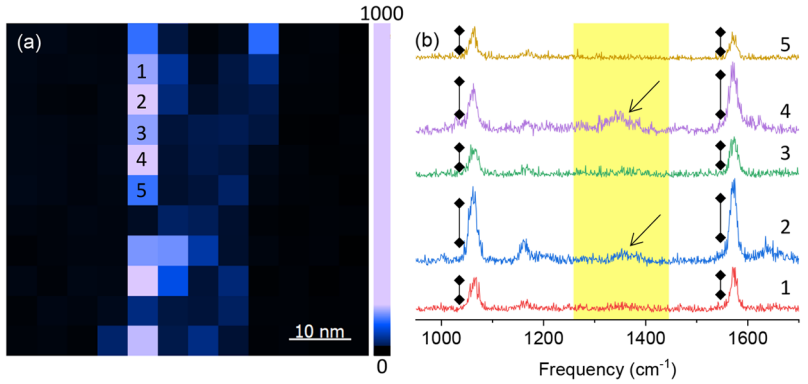

Figure 4. Zoomed in TERS image, tracing the edge of a silver nanocube (centered to the left of the image shown in panel a). Several pixels are enumerated in (a) and plotted in (b). They show the prevalence of the CO_2-bound vs S-bound MBA. See text for more discussion.

using a CCD camera (Andor, Newton EMCCD) coupled to a spectrometer (Andor, Shamrock 500) equipped with a 300 l/mm grating blazed at 550 nm.

Density functional theory calculations were performed using a local version of NWChem.[22] Geometry optimization and Raman spectral simulations were performed at the PBE/def2-TZVP level of theory.

■ ASSOCIATED CONTENT

Supporting Information

The Supporting Information is available free of charge at https://pubs.acs.org/doi/10.1021/acs.jpclett.1c00661.

Simulations of molecular orientation-dependent TERS from MBA; simulated spectra of MBA vs the S-bound MBA-Ag complex; vector representation of the 1359 cm^{-1} mode in the Ag_{20}-MBA complex (PDF)

■ AUTHOR INFORMATION

Corresponding Author

Patrick Z. El-Khoury − *Physical Sciences Division, Pacific Northwest National Laboratory, Richland, Washington 99352, United States;* orcid.org/0000-0002-6032-9006; Email: patrick.elkhoury@pnnl.gov

Authors

Matthew Gabel − *Department of Physics and Astronomy, Washington State University, Pullman, Washington 99164, United States*

Brian T. O'Callahan − *Earth and Biological Sciences Division, Pacific Northwest National Laboratory, Richland, Washington 99352, United States;* orcid.org/0000-0001-9835-3207

Chloe Groome − *Department of Materials Science and Engineering, University of California, Irvine, Irvine, California 92697-2575, United States*

Chih-Feng Wang − *Physical Sciences Division, Pacific Northwest National Laboratory, Richland, Washington 99352, United States;* orcid.org/0000-0002-3085-6614

Regina Ragan − *Department of Materials Science and Engineering, University of California, Irvine, Irvine, California 92697-2575, United States;* orcid.org/0000-0002-8694-5683

Yi Gu − *Department of Physics and Astronomy, Washington State University, Pullman, Washington 99164, United States*

Complete contact information is available at: https://pubs.acs.org/10.1021/acs.jpclett.1c00661

Notes

The authors declare the following competing financial interest(s): Y.G. is an advisor for Klar Scientific LLC.

■ ACKNOWLEDGMENTS

M.G. and C.G. acknowledge support from the United States National Science Foundation through CMMI-1930769 (Y.G.) and CBET-1926612 (R.R.). B.T.O. and C.F.W. were supported by the US Department of Energy (DOE), Office of Science, Office of Biological and Environmental Research through the bioimaging technology development program. P.Z.E. was supported by the US DOE, Office of Science, Office of Basic Energy Sciences, Division of Chemical Sciences, Geosciences & Biosciences. This work was performed at Pacific Northwest National Laboratory (PNNL). PNNL is operated by Battelle Memorial Institute for the United States Department of Energy under DOE contract number DE-AC05-76RL1830.

■ REFERENCES

(1) El-Khoury, P. Z.; Schultz, Z. D. From SERS to TERS and Beyond: Molecules as Probes of Nanoscopic Optical Fields. *J. Phys. Chem. C* **2020**, *124*, 27267−27275.

(2) Graham, D.; Moskovits, M.; Tian, Z.-Q. SERS − Facts, Figures and the Future. *Chem. Soc. Rev.* **2017**, *46*, 3864−3865.

(3) Stöckle, R. M.; Suh, Y. D.; Deckert, V.; Zenobi, R. Nanoscale Chemical Analysis by Tip-Enhanced Raman Spectroscopy. *Chem. Phys. Lett.* **2000**, *318*, 131−136.

(4) Wang, X.; Huang, S.-C.; Huang, T.-X.; Su, H.-S.; Zhong, J.-H.; Zeng, Z.-C.; Li, M.-H.; Ren, B. Tip-Enhanced Raman Spectroscopy for Surfaces and Interfaces. *Chem. Soc. Rev.* **2017**, *46*, 4020−4041.

(5) El-Khoury, P. Z.; Aprà, E. Spatially Resolved Mapping of Three-Dimensional Molecular Orientations with ∼ 2 nm Spatial Resolution through Tip-Enhanced Raman Scattering. *J. Phys. Chem. C* **2020**, *124*, 17211−17217.

(6) Lombardi, J. R.; Birke, R. L. The Theory of Surface-Enhanced Raman Scattering. *J. Chem. Phys.* **2012**, *136*, 144704.

(7) Wang, C.-F.; Cheng, Z.; O'Callahan, B. T.; Crampton, K. T.; Jones, M. R.; El-Khoury, P. Z. Tip-Enhanced Multipolar Raman Scattering. *J. Phys. Chem. Lett.* **2020**, *11*, 2464−2469.

(8) Sprague-Klein, E. A.; McAnally, M. O.; Zhdanov, D. V.; Zrimsek, A. B.; Apkarian, V. A.; Seideman, T.; Schatz, G. C.; Van Duyne, R. P. Observation of Single Molecule Plasmon-Driven Electron Transfer in Isotopically Edited 4,4′-Bipyridine Gold Nanosphere Oligomers. *J. Am. Chem. Soc.* **2017**, *139*, 15212−15221.

(9) Zrimsek, A. B.; Chiang, N.; Mattei, M.; Zaleski, S.; McAnally, M. O.; Chapman, C. T.; Henry, A.-I.; Schatz, G. C.; Van Duyne, R. P. Single-Molecule Chemistry with Surface- and Tip-Enhanced Raman Spectroscopy. *Chem. Rev.* **2017**, *117*, 7583−7613.
(10) Chulhai, D. V.; Jensen, L. Simulating Surface-Enhanced Raman Optical Activity Using Atomistic Electrodynamics-Quantum Mechanical Models. *J. Phys. Chem. A* **2014**, *118*, 9069−9079.
(11) Kurouski, D.; Zaleski, S.; Casadio, F.; Van Duyne, R. P.; Shah, N. C. Tip-Enhanced Raman Spectroscopy (TERS) for in Situ Identification of Indigo and Iron Gall Ink on Paper. *J. Am. Chem. Soc.* **2014**, *136*, 8677−8684.
(12) Ho, C.-H.; Lee, S. SERS and DFT Investigation of the Adsorption Behavior of 4-Mercaptobenzoic Acid on Silver Colloids. *Colloids Surf., A* **2015**, *474*, 29−35.
(13) Michota, A.; Bukowska, J. Surface-Enhanced Raman Scattering (SERS) of 4-Mercaptobenzoic Acid on Silver and Gold Substrates. *J. Raman Spectrosc.* **2003**, *34*, 21−25.
(14) Suh, J. S.; Kim, J. Three Distinct Geometries of Surface-Adsorbed Carboxylate Groups. *J. Raman Spectrosc.* **1998**, *29*, 143−148.
(15) Ghosh, A.; Ahuja, T.; Chaudhari, K.; Pradeep, T. Probing Subtle Changes in Molecular Orientations Using Ambient Electrospray Deposition Raman Spectroscopy (AESD RS). *J. Phys. Chem. C* **2020**, *124*, 16644−16651.
(16) Bhattarai, A.; Novikova, I. V.; El-Khoury, P. Z. Tip-Enhanced Raman Nanographs of Plasmonic Silver Nanoparticles. *J. Phys. Chem. C* **2019**, *123*, 27765−27769.
(17) Aprà, E.; Bhattarai, A.; El-Khoury, P. Z. Gauging Molecular Orientation through Time Domain Simulations of Surface-Enhanced Raman Scattering. *J. Phys. Chem. A* **2019**, *123*, 7142−7147.
(18) Wang, C.-F.; O'Callahan, B. T.; Kurouski, D.; Krayev, A.; El-Khoury, P. Z. The Prevalence of Anions at Plasmonic Nanojunctions: A Closer Look at p-Nitrothiophenol. *J. Phys. Chem. Lett.* **2020**, *11*, 3809−3814.
(19) Noda, I.; Ozaki, Y. *Two-Dimensional Correlation Spectroscopy: Applications in Vibrational and Optical Spectroscopy*; Wiley, 2004.
(20) Wang, C.-F.; O'Callahan, B. T.; Kurouski, D.; Krayev, A.; Schultz, Z. D.; El-Khoury, P. Z. Suppressing Molecular Charging, Nanochemistry, and Optical Rectification in the Tip-Enhanced Raman Geometry. *J. Phys. Chem. Lett.* **2020**, *11*, 5890−5895.
(21) O'Callahan, B. T.; Bhattarai, A.; Schultz, Z. D.; El-Khoury, P. Z. Power-Dependent Dual Analyte Tip-Enhanced Raman Spectral Imaging. *J. Phys. Chem. C* **2020**, *124*, 15454−15459.
(22) Valiev, M.; Bylaska, E. J.; Govind, N.; Kowalski, K.; Straatsma, T. P.; Van Dam, H. J. J.; Wang, D.; Nieplocha, J.; Apra, E.; Windus, T. L.; de Jong, W. A. NWChem: A Comprehensive and Scalable Open-Source Solution for Large Scale Molecular Simulations. *Comput. Phys. Commun.* **2010**, *181*, 1477−1489.

https://doi.org/10.1021/acs.jpclett.1c00661
J. Phys. Chem. Lett. 2021, 12, 3586−3590